Monthly Notices of the ROYAL ASTRONOMICAL SOCIETY

MNRAS **477,** 2406–2418 (2018)
Advance Access publication 2018 March 17

doi:10.1093/mnras/sty596

A local model of warped magnetized accretion discs

J. B. Paris★ and G. I. Ogilvie

Department of Applied Mathematics and Theoretical Physics, Centre for Mathematical Sciences, University of Cambridge, Wilberforce Road, Cambridge CB3 0WA, UK

Accepted 2018 February 27. Received 2018 February 26; in original form 2017 March 10

ABSTRACT

We derive expressions for the local ideal magnetohydrodynamic (MHD) equations for a warped astrophysical disc using a warped shearing box formalism. A perturbation expansion of these equations to first order in the warping amplitude leads to a linear theory for the internal local structure of magnetized warped discs in the absence of magnetorotational instability (MRI) turbulence. In the special case of an external magnetic field oriented normal to the disc surface, these equations are solved semi-analytically via a spectral method. The relatively rapid warp propagation of low-viscosity Keplerian hydrodynamic warped discs is diminished by the presence of a magnetic field. The magnetic tension adds a stiffness to the epicyclic oscillations, detuning the natural frequency from the orbital frequency and thereby removing the resonant forcing of epicyclic modes characteristic of hydrodynamic warped discs. In contrast to a single hydrodynamic resonance, we find a series of Alfvénic-epicyclic modes which may be resonantly forced by the warped geometry at critical values of the orbital shear rate q and magnetic field strength. At these critical points large internal torques are generated and anomalously rapid warp propagation occurs. As our treatment omits MRI turbulence, these results are of greatest applicability to strongly magnetized discs.

Key words: accretion, accretion discs – MHD.

1 INTRODUCTION

Warped astrophysical discs are discs in which the orientation of the orbital plane is dependent on the radius. These warps may be produced by a wide variety of sources, such as Lense–Thirring torques (Bardeen & Petterson 1975) from a central misaligned spinning black hole or the torques due to a misaligned companion object in a binary star system (Terquem & Papaloizou 2000). Theoretical considerations and observations revealing the existence of warped discs in several systems, such as the X-ray binary Her X-1 and the galactic nucleus of NGC 4258 (M106) (Miyoshi et al. 1995), have historically motivated the study of warped accretion disc dynamics.

Early theoretical studies (Bardeen & Petterson 1975; Hatchett, Begelman & Sarazin 1981) found evolutionary equations for the shape of a warped disc and suggested that the warp would diffuse on a viscous time-scale inversely proportional to α, where α is the Shakura–Sunyaev viscosity parameter. These models were challenged by Papaloizou & Pringle (1983) who determined that the prior models failed to appropriately recognize the importance of internal flows within the disc and consequently did not conserve angular momentum.

Papaloizou & Lin (1995) and earlier works showed that warps in inviscid Keplerian discs propagate as bending waves at a fraction of the sound speed. The fully non-linear theory for the diffusive regime in Keplerian discs and for the slower bending waves in non-Keplerian discs was derived by Ogilvie (1999). In that work it was shown that warped hydrodynamic discs exhibit resonant behaviour when the disc is Keplerian and the warp is small.

More recently, Ogilvie & Latter (2013a) have shown that the non-linear hydrodynamic theory of Ogilvie (1999) can be derived by separating the global and local aspects of a warped thin disc. The global evolution of the mass distribution and the shape of the disc can be deduced from the (vectorial) conservation of angular momentum, provided that the internal torque is known. The internal torque can be calculated from time-averaged quantities in a local model, which is constructed around a reference point that follows a circular orbit through a warped disc and experiences a geometry that oscillates at the orbital frequency, thereby generalizing the well-known shearing sheet or box. The simplest solutions in the warped shearing box are laminar internal flows that oscillate at the orbital frequency; these are driven by a radial pressure gradient that arises from the warped geometry and the vertical stratification of the disc. Owing to the coincidence of the orbital and epicyclic frequency in a Keplerian disc, this forcing may result in fast internal flows for even comparatively small warps. Such flows generate correspondingly large internal torques, leading to the rapid propagation of the warp.

There are many situations in which these hydrodynamic models are not valid. Astrophysical discs are often threaded by large or small-scale magnetic fields thought to be important in the

★ E-mail: jp514@cam.ac.uk

© 2018 The Author(s)
Published by Oxford University Press on behalf of the Royal Astronomical Society

Downloaded from https://academic.oup.com/mnras/article-abstract/477/2/2406/4942271
by University of Cambridge user
on 18 June 2018

formation of jet outflows (Blandford & Payne 1982) and the transport of angular momentum via the magnetorotational instability (MRI; Balbus & Hawley 1991). These magnetized discs may be created, for example, by dragging in significant amounts of magnetic flux during disc formation as is thought to be the case for protostellar discs (Lewis & Bate 2017). It is therefore likely that there exist many disc systems in which both large-scale magnetic fields and the warped geometry will have important effects on disc dynamics. Despite this, the study of warped discs and the study of magnetized discs have generally been done in relative isolation. With a few notable exceptions, comparatively little attention has been given to the complex interplay between these two aspects of accretion disc physics.

From a computational perspective, it has been difficult to resolve warp evolution in large-scale magnetohydrodynamic (MHD) simulations. This difficulty lies in the vast separation between the time-scale of MHD turbulence, which requires a time-step very short relative to the orbital period, and the warp evolution time-scale which is usually far longer than the orbital period. However, a limited body of work on warped magnetized discs does exist. Fragile et al. (2007) performed one of the first 3D MHD simulations of a relatively thick tilted disc around a rotating black hole. The radial extent of the simulation was unfortunately not large enough to capture significant disc warping. The simulations of tilted discs around stellar objects of Lovelace & Romanova (2014) and Sheikhnezami & Fendt (2015) on the other hand were concerned primarily with Rossby wave trapping and jet launching respectively, providing relatively little insight on the warp evolution process.

The global 3D MHD simulations of a warped disc recently performed by Sorathia, Krolik & Hawley (2013b) were among the first to resolve shape evolution in a magnetized accretion disc. In that work it was argued that neither the bending wave nor the diffusion models of warp propagation were adequate to properly describe the observed warp propagation. Qualitative differences between the hydrodynamic (Sorathia, Krolik & Hawley (2013a) and MHD warped disc simulations (most notably a distinctively sharper warp profile in the hydrodynamic case) were also observed. Although the departure from standard hydrodynamic warped disc theory was partially explained through non-linear damping effects, the magnetohydrodynamic aspect was clearly recognized and arguments involving the MRI-driven background turbulence and anisotropic viscosities were presented to rationalize the observed warp propagation. These results raise questions about the applicability of certain aspects of hydrodynamic warped disc theory (especially the neat separation of discs into 'diffusive' or 'bending wave' regimes) to magnetized discs. A contrary view has been presented by Nealon et al. (2016), who found that the results of a similar MHD simulation by Krolik & Hawley (2015) – which does however begin with a weaker mean magnetic field – could be quite accurately reproduced using a hydrodynamic simulation with an alpha viscosity. Continued interest in Bardeen–Petterson alignment has stimulated the production of a number of recent warped magnetized disc simulations such as Zhuravlev et al. (2014). The advent of 3D MHD simulations of this kind necessitates the development of a corresponding theory of warp propagation in magnetized discs in order to explain the salient features of these simulations.

Bending instabilities in a magnetized warped disc subject to an inclined dipole field were studied in a vertically integrated manner by Agapitou, Papaloizou & Terquem (1997). Lai (1999) investigated warping in a magnetized disc due to an inclined dipole, but did not include the effects of the warped disc geometry itself on the disc response. Terquem & Papaloizou (2000) included this effect and were able to determine the global warped disc structure for a variety of magnetic field configurations. However, none of these models considered the potentially dramatic effects of driven internal flows such as those described by Ogilvie & Latter (2013a) in hydrodynamic warped discs. The work presented in this paper attempts to analyse whether these dramatic resonantly driven flows and their associated large torques exist in magnetized warped discs, and if so, what consequences they would have for the evolution of the warp.

The problem of a magnetized warped disc presents a number of different issues and regimes, only some of which can be addressed in this paper. If the disc is threaded by a large-scale magnetic field, the warping of the disc will affect the structure of this external field and will generally produce torques on the disc that will cause the warp to evolve. This aspect of the problem is global in character and can be studied only to a limited extent using the local model considered in this paper. A magnetic field will also affect the interior dynamics of the disc. If it is sufficiently weak, it can cause the MRI, which can produce MHD turbulence. The occurrence of the MRI in a warped disc, its effect on the internal flows and torques, and its interaction with the hydrodynamic instability studied by Ogilvie & Latter (2013b) could be usefully studied in the local model of the warped shearing box. The launching of outflows from a magnetized disc can be studied to some extent using local models (Ogilvie 2012) and the interaction of that problem with a warp also deserves investigation. In this paper we take a useful first step by calculating the laminar internal flows in a warped disc threaded by a magnetic field in ideal MHD. The laminar solutions are of most direct relevance when the field is sufficiently strong to suppress the MRI.

In Section 2 we employ the warped shearing box model developed by Ogilvie & Latter (2013a) to express the fully non-linear local ideal MHD equations in a reference frame comoving with a fluid element in the warped disc mid-plane. In Section 3 we consider one-dimensional laminar solutions to these equations, and by expanding linearly in warp amplitude about an equilibrium solution, a system of first-order differential equations is found for the internal structure of the disc.

In Section 4 we consider the special case of a warped disc threaded by a magnetic field perpendicular to the disc mid-plane. A solution to this particular case is found via a spectral method. The unique features of magnetized warped disc dynamics are discussed. In Section 5 we outline two numerical procedures that are used to check the results of the spectral method. In Section 6 the results of the paper are discussed and summarized.

2 THE LOCAL MODEL OF A WARPED DISC

2.1 The warped shearing box

We restrict ourselves to circular warped discs (as opposed to elliptical discs) due to their relative simplicity. Ogilvie (1999) showed that a circular warped disc may be mathematically described by a radially dependent vector $\boldsymbol{l}(r,t)$ defined to be perpendicular to the orbital plane of the fluid at radius r. The radial dependence of the orbital plane causes a warping in the disc geometry, as can be seen in Fig. 1. For this class of accretion disc, only the dimensionless warp amplitude ψ defined by $\psi = r\left|\frac{\partial \boldsymbol{l}}{\partial r}\right|$ is necessary to specify the local geometry of the warped disc. The physical significance of the warping parameter ψ can be clearly seen in Fig. 2.[1]

[1] Figs 1 and 2 are derived from figures originally published in Ogilvie & Latter (2013a).

Downloaded from https://academic.oup.com/mnras/article-abstract/477/2/2406/4942271
by University of Cambridge user
on 18 June 2018

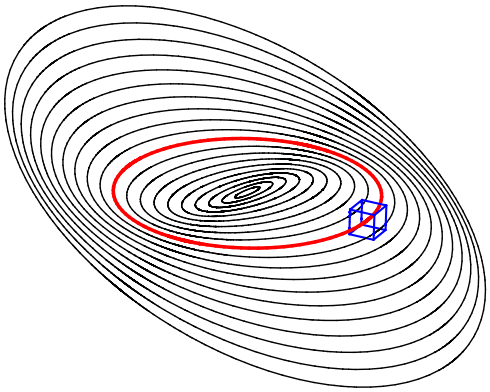

Figure 1. A warped disc, viewed as a collection of tilted rings. As discussed in Section 2.1, a local frame (the blue box) is centred on a point that follows the red reference orbit.

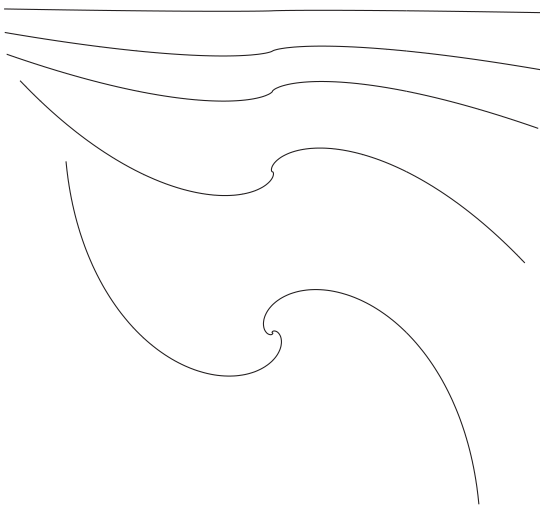

Figure 2. A side-on view of untwisted warps with constant warp amplitudes $\psi = 0.01$ (top), 0.1, 0.2, 0.5, and 1 (bottom).

Local models of unwarped accretion discs are typically constructed around a reference point in the mid-plane of the disc co-orbiting with the surrounding fluid. A Cartesian coordinate system can be imposed with the origin at this reference point and the axes rotating at the orbital frequency such that the x-direction is radial, the y-direction is azimuthal, and the z-direction is perpendicular to the disc mid-plane. There is a shearing flow within the box due the differential rotation of the disc; consequently such models are often called 'shearing box' models.

An analogous construction is the 'warped shearing box', introduced in Ogilvie & Latter (2013a). In warped shearing box models, a Cartesian coordinate system is constructed around a reference point in the mid-plane of a warped accretion disc as shown in Fig. 1. The warped shearing box is represented by the non-orthogonal primed coordinates (t', x', y', z') chosen to compensate for the local geometry of the warped disc. These are related to the Cartesian coordinate system (t, x, y, z) comoving with the fluid via expressions (1)–(4) below, where $q \equiv -\frac{\mathrm{d}\ln\Omega}{\mathrm{d}\ln r}$ is the orbital shear rate of the disc in question and Ω is the orbital frequency at the reference radius.

We define z' such that the surface $z' = 0$ corresponds to the mid-plane of the warped disc and the z'-axis is normal to the disc mid-plane rather than normal to the orbital plane. The definition of y' simply takes into account the shear due to the differential rotation, where q is assumed to be 3/2 for a Keplerian disc. The relative velocities $\boldsymbol{v}$ are constructed to remove the expected azimuthal velocity changes due to shear or the vertical velocity changes due to the warped geometry of the disc.

$$t' = t, \tag{1}$$

$$x' = x, \tag{2}$$

$$y' = y + q\Omega t x, \tag{3}$$

$$z' = z + \psi x \cos(\Omega t). \tag{4}$$

In such coordinates, it is important to note that

$$\partial_t = \partial_{t'} + q\Omega x \partial_{y'} - \psi\Omega x \sin(\Omega t)\partial_{z'}, \tag{5}$$

$$\partial_x = \partial_{x'} + q\Omega t \partial_{y'} + \psi \cos(\Omega t)\partial_{z'}, \tag{6}$$

$$\partial_y = \partial_{y'}, \tag{7}$$

$$\partial_z = \partial_{z'}, \tag{8}$$

and relative velocities are defined such that

$$v_x = u_x, \tag{9}$$

$$v_y = u_y + q\Omega x, \tag{10}$$

$$v_z = u_z - \psi\Omega x \sin(\Omega t). \tag{11}$$

2.2 The non-linear MHD equations in a warped disc

Having defined the coordinate system of the warped shearing box, we may now express the full non-linear local MHD equations in these coordinates.

2.2.1 *The physical equations*

The momentum equation expressed in a coordinate system corotating with the reference orbit is

$$\rho\left(\frac{D\boldsymbol{u}}{Dt} + 2\Omega\mathbf{e}_z \wedge \boldsymbol{u}\right) = -\rho\nabla\Phi - \nabla p + \boldsymbol{J} \wedge \boldsymbol{B}, \tag{12}$$

where the effective potential due to a central gravitational force and the rotating frame is given by

$$\Phi = \frac{1}{2}\Omega^2(z^2 - 2qx^2) \tag{13}$$

and the Lorentz force in ideal MHD is expressed as

$$\boldsymbol{J} \wedge \boldsymbol{B} = \frac{1}{\mu_0}(\boldsymbol{B}\cdot\nabla)\boldsymbol{B} - \frac{1}{2\mu_0}\nabla\boldsymbol{B}^2. \tag{14}$$

The induction equation in ideal MHD is given by

$$\frac{\partial\boldsymbol{B}}{\partial t} = \nabla \wedge (\boldsymbol{u} \wedge \boldsymbol{B}) = \boldsymbol{B}\cdot\nabla\boldsymbol{u} - \boldsymbol{u}\cdot\nabla\boldsymbol{B} - \boldsymbol{B}(\nabla\cdot\boldsymbol{u}), \tag{15}$$

while the continuity equation gives

$$\frac{\partial\rho}{\partial t} + \nabla\cdot(\rho\boldsymbol{u}) = 0. \tag{16}$$

For simplicity the disc is assumed to be isothermal with uniform sound speed c_s, implying

$$p = c_s^2\rho. \tag{17}$$

Downloaded from https://academic.oup.com/mnras/article-abstract/477/2/2406/4942271
by University of Cambridge user
on 18 June 2018

Rather than expressing the full MHD equations in terms of the vector components perpendicular to the orbital plane, such as v_z and B_z, it will be more convenient to consider the vector components perpendicular to the disc mid-plane as defined by $v_{z'} = v_z + \psi\cos(\Omega t)v_x$, $B_{z'} = B_z + \psi\cos(\Omega t)B_x$ (in fact, these are contravarient vector components in the warped shearing coordinate system). The full non-linear MHD equations are then given by

$$\frac{Dv_x}{Dt'} - 2\Omega v_y = -\frac{1}{\rho}[\partial_{x'} + q\Omega t'\partial_{y'} + \psi\cos(\Omega t')\partial_{z'}]\Pi + \frac{1}{\mu_0\rho}(\boldsymbol{B}'\cdot\boldsymbol{\nabla})B_x, \tag{18}$$

$$\frac{Dv_y}{Dt'} + (2-q)\Omega v_x = -\frac{1}{\rho}\partial_{y'}\Pi + \frac{1}{\mu_0\rho}(\boldsymbol{B}'\cdot\boldsymbol{\nabla})B_y, \tag{19}$$

$$\frac{Dv_{z'}}{Dt'} = -2\psi\Omega\sin(\Omega t')v_x - \Omega^2 z' + 2\Omega\psi\cos(\Omega t')v_y - \frac{\gamma^2}{\rho}\partial_{z'}\Pi - \frac{1}{\rho}\psi\cos(\Omega t')(\partial_{x'} + q\Omega t'\partial_{y'})\Pi + \frac{1}{\mu_0\rho}(\boldsymbol{B}'\cdot\boldsymbol{\nabla})B_{z'}, \tag{20}$$

$$\frac{\partial B_x}{\partial t'} = \boldsymbol{B}'\cdot\nabla v_x - (\nabla\cdot\boldsymbol{v}')B_x - \boldsymbol{v}'\cdot\nabla B_x, \tag{21}$$

$$\frac{\partial B_y}{\partial t'} = -q\Omega B_x + \boldsymbol{B}'\cdot\nabla v_y - (\nabla\cdot\boldsymbol{v}')B_y - \boldsymbol{v}'\cdot\nabla B_y, \tag{22}$$

$$\frac{\partial B_{z'}}{\partial t'} = \boldsymbol{B}'\cdot\nabla v_{z'} - (\nabla\cdot\boldsymbol{v}')B_{z'} - \boldsymbol{v}'\cdot\nabla B_{z'}, \tag{23}$$

$$\nabla\cdot\boldsymbol{B}' = 0, \tag{24}$$

$$\partial_{t'}\rho + \rho(\nabla\cdot\boldsymbol{v}') + \boldsymbol{v}'\cdot\nabla\rho = 0, \tag{25}$$

where

$$\frac{D}{Dt'} = \partial_{t'} + \boldsymbol{v}'\cdot\nabla, \tag{26}$$

$$\boldsymbol{v}'\cdot\nabla = v_x\partial_{x'} + (v_y + q\Omega t' v_x)\partial_{y'} + v_{z'}\partial_{z'}, \tag{27}$$

$$\nabla\cdot\boldsymbol{v}' = \partial_{x'}v_x + \partial_{y'}(v_y + q\Omega t' v_x) + \partial_{z'}v_{z'}, \tag{28}$$

$$\boldsymbol{B}'\cdot\nabla = B_x\partial_{x'} + (B_y + q\Omega t' B_x)\partial_{y'} + B_{z'}\partial_{z'}, \tag{29}$$

$$\nabla\cdot\boldsymbol{B}' = \partial_{x'}B_x + \partial_{y'}(B_y + q\Omega t' B_x) + \partial_{z'}B_{z'}, \tag{30}$$

total pressure $\Pi \equiv c_s^2\rho + \frac{\mathbf{B}^2}{2\mu_0}$ and $\gamma^2 \equiv 1 + \psi^2\cos^2(\Omega t')$.

This system of equations is horizontal homogeneous as it does not refer explicitly to x' or y', and so is compatible with periodic horizontal boundary conditions. In order to solve this system of equations, boundary conditions far from the disc mid-plane must be imposed. More specifically limiting magnetic field values, along with a condition on material inflow/outflow, must be prescribed.

2.2.2 *The validity of the local model*

It is imperative that we keep track of the assumptions made to derive these equations. First, we have assumed an isothermal gas for simplicity. Perhaps more subtly there is also an implicit separation of scales in the formulation of these equations. The warp, expressed by the warp amplitude ψ, is assumed to be independent of time. This reflects the assumption that the warp propagates on a time-scale far longer than the orbital time-scale ($|\frac{\mathrm{d}\psi}{\mathrm{d}t}| \ll \Omega\psi$).

At first glance it may seem curious that the warp amplitude is a fixed parameter given that this model is intended partly for the study of warp propagation. However, there is no contradiction here. The warp amplitude determines the internal dynamics of the disc on the fast orbital time-scale. An internal torque is generated by the internal flows driven by the warp (as discussed in section 4.2), which can be calculated. In principle the warp could then be allowed us to vary on a slower time-scale in a manner consistent with the torques acting upon that annulus of the disc. In practice, however, we can deduce the evolution of the warp from the calculated internal torque and the conservation of angular momentum. In this way, warp propagation may be investigated in the local model without an explicitly time-dependent warp amplitude.

Ogilvie & Latter (2013a) displayed that the hydrodynamic warped shearing box is indeed capable of replicating the results of the global asymptotic theory of warped discs (Ogilvie 1999), validating the local approach. An investigation further exploring the connection between the global and local theory of warped discs is forthcoming.

Other challenges may be levelled at this approach to warped disc dynamics. If one were to investigate solutions to these equations that are either one-dimensional or have periodic radial boundaries, one would require the structure of the warp to vary on a length scale much greater than the radial excursion of fluid elements over the period of an orbit. If this were not the case, then the radial variation of the warp amplitude would affect the internal structure of the disc and it would be impossible to characterize a region of the disc by a single value for the warp amplitude. Hence the warped shearing box would be unable to appropriately model a disc with extreme radial variations in warp amplitude. If the warp varies on the length scale of the disc radius this condition simplifies to $|\boldsymbol{v}| \ll \Omega R$, or equivalently the relative velocity must be much less than the orbital velocity.

Additionally, the presence of a global magnetic field implies that in some sense the transport of angular momentum may not be truly local as is the case for hydrodynamic discs, but rather angular momentum may be communicated non-locally via magnetic stresses to other parts of the disc. This issue enters the local model via several unspecified boundary terms (see Section 3.2.2). This topic is discussed in greater detail in the follow-up paper.

3 ONE-DIMENSIONAL SOLUTIONS

3.1 Non-linear 1D MHD equations

Having derived the fully non-linear local MHD equations we proceed by looking for the simplest solutions for the disc structure. The warped shearing box was designed such that the MHD equations do not explicitly contain x' or y', and are hence horizontally homogeneous. We therefore start by seeking solutions that are independent of x' and y'. All physical quantities are taken to be functions of z' and t' alone, and the MHD equations reduce to a set of 1D equations. Recall that the oscillatory time-dependence of quantities in the local model corresponds to their azimuthal dependence in a global description (see Fig. 1). We note that such a laminar flow excludes the possibility of turbulence, most notably MRI turbulence.

Downloaded from https://academic.oup.com/mnras/article-abstract/477/2/2406/4942271
by University of Cambridge user
on 18 June 2018

3.1.1 Scaling

$B_{z'}$, as shown in the following section, is a constant of the motion and therefore can be used as a scaling parameter. Using this convention the above set of equations (18)–(30) can be made dimensionless via the following scaling relations:

$$\widehat{t} = \Omega t, \tag{31}$$

$$\widehat{z}' = \frac{z'\Omega}{c_s}, \tag{32}$$

$$\widehat{v}_i = v_i/c_s, \tag{33}$$

$$\widehat{\rho} = \frac{\rho c_s}{\Sigma\Omega}, \tag{34}$$

$$\widehat{B}_{z'} = \frac{B_{z'}}{\sqrt{\mu_0 \Sigma c_s \Omega}}, \tag{35}$$

$$\widehat{B}_x = \frac{B_x}{B_{z'}}, \tag{36}$$

where c_s is the isothermal sound speed, Σ is the vertically integrated surface density of the disc, and all other terms maintain their previous definitions.

From this point onwards all physical quantities will be scaled as shown above and the circumflexes will be removed. The one-dimensional non-linear MHD equations are hence given by

$$\frac{Dv_x}{Dt'} - 2v_y = -\frac{\psi\cos(t')}{\rho}\partial_{z'}\rho + \frac{B_{z'}^2}{\rho}\{\gamma^2[\partial_{z'}B_x - \psi\cos(t')B_x\partial_{z'}B_x] - \psi\cos(t')B_y\partial_{z'}B_y\}, \tag{37}$$

$$\frac{Dv_y}{Dt'} = -(2-q)v_x + \frac{B_{z'}^2}{\rho}\partial_{z'}B_y, \tag{38}$$

$$\frac{Dv_{z'}}{Dt'} = -2\psi\sin(t')v_x - z' + 2\psi\cos(t')v_y - \frac{\gamma^2}{\rho}\partial_{z'}\rho + \frac{B_{z'}^2\gamma^2}{\rho}[-\gamma^2 B_x\partial_{z'}B_x + \psi\cos(t')\partial_{z'}B_x - B_y\partial_{z'}B_y], \tag{39}$$

$$\frac{\partial\rho}{\partial t'} + \partial_{z'}(\rho v_{z'}) = 0, \tag{40}$$

$$\frac{\partial B_x}{\partial t'} = \partial_{z'}v_x - v_{z'}\partial_{z'}B_x - B_x\partial_{z'}v_{z'}, \tag{41}$$

$$\frac{\partial B_y}{\partial t'} = \partial_{z'}v_y - qB_x - v_{z'}\partial_{z'}B_y - B_y\partial_{z'}v_{z'}, \tag{42}$$

$$\frac{\partial B_{z'}}{\partial t'} = 0, \tag{43}$$

$$\frac{\partial B_{z'}}{\partial z'} = 0, \tag{44}$$

where $\frac{D}{Dt'} = \partial_{t'} + v_{z'}\partial_{z'}$ and $\gamma^2 \equiv 1 + \psi^2\cos^2(t')$.

3.1.2 Properties of the non-linear 1D MHD equations

Some general comments can be made at this stage. The final two equations (43)–(44) reveal an important property of warped magnetized accretion discs. The magnetic field component perpendicular to the disc mid-plane, $B_{z'}$, is independent of both time and height above the mid-plane. This is a consequence of magnetic flux conservation under the assumption of horizontal uniformity. The magnetic field perpendicular to the disc mid-plane is therefore advected with the fluid and a constant of the motion, while the other magnetic field components are not. Thus the use of $B_{z'}$ as a scaling parameter is justified.

In a standard unwarped accretion disc there is an azimuthal symmetry present in the equations of motion. With suitable boundary conditions and in the absence of a symmetry-breaking process, there is therefore an azimuthal symmetry in all physical quantities. Although this axisymmetry is broken in a warped disc, equations (37)–(44) reveal that a point symmetry still exists. This point symmetry could be described as a reflection in the local disc mid-plane followed by a rotation by π radians. For example, for a scalar quantity $f(z', t')$ this transformation can be represented by the operator $\widehat{T}$ such that

$$\widehat{T}f(z', t') = f(-z', t' + \pi). \tag{45}$$

For vector quantities, the vector components parallel to the disc plane are invariant under transformation $\widehat{T}$ and the vector components perpendicular to the disc surface are inverted. For pseudo-vectors, the opposite is true; pseudo-vector components parallel to the disc surface are inverted, while pseudo-vector components perpendicular to the disc surface are invariant.

This symmetry can be proven by making the appropriate simultaneous transformation in the warped disc MHD equations: $\{z' \to -z', t' \to t' + \pi, \rho \to \rho, v_x \to v_x, v_y \to v_y, v_{z'} \to -v_{z'}, B_x \to -B_x, B_y \to -B_y, B_{z'} \to B_{z'}\}$. This transformation leaves equations (37)–(44) invariant, and is therefore a symmetry of the system. The existence of this symmetry is not only of physical interest but is of practical use in the numerical work described in sections 4 and 5.

3.2 Perturbation analysis of the warped disc MHD equations

In the previous section we found a set of one-dimensional MHD equations for the vertical structure of a magnetized warped disc. We proceed by linearizing these equations with respect to the warp amplitude ψ. The solutions found by this method will be valid only for small warps ($\psi \ll 1$).

3.2.1 The unwarped solution

The equilibrium state is chosen to be an unwarped disc such that $B_y = v_x = v_{z'} = 0$ and there is no jet outflow for simplicity (Ogilvie 1997). This represents an unwarped accretion disc with a poloidal magnetic field and a purely azimuthal velocity.

The unwarped disc is described by three variables $\{\rho_0, B_{x0}, v_{y0}\}$ which satisfy the following set of equations:

$$2v_{y0} + \frac{B_{z'}^2}{\rho_0}d_{z'}B_{x0} = 0, \tag{46}$$

$$z' + \frac{1}{\rho_0}d_{z'}\rho_0 + \frac{B_{z'}^2}{\rho_0}B_{x0}d_{z'}B_{x0} = 0, \tag{47}$$

$$d_{z'}v_{y0} - qB_{x0} = 0. \tag{48}$$

The following three associated boundary conditions must also be satisfied:

$$B_{x0}|_{z'\to\infty} = \tan i, \tag{49}$$

$$B_{x0}(0) = 0, \tag{50}$$

Downloaded from https://academic.oup.com/mnras/article-abstract/477/2/2406/4942271
by University of Cambridge user
on 18 June 2018

and

$$\int_{-\infty}^{\infty} \rho_0(z')\,\mathrm{d}z' = 1. \tag{51}$$

The first condition states that the inclination angle i of the poloidal magnetic field has to be specified at large z'. We only consider $i < 30^\circ$, as an inclination angle in excess of this value produces a jet outflow (Blandford & Payne 1982). The second condition is a result of the odd symmetry of B_{x0} in z', and the final condition normalizes the surface density of the disc.

3.2.2 *The MHD equations to first order*

Through inspection of equations (37)–(44) and comparison with the hydrodynamic solutions found by Ogilvie & Latter (2013a), all first-order physical quantities can be expected to vary sinusoidally throughout the orbit. More specifically, the following time-dependence is consistent with the MHD equations (37)–(44) to first order in warp amplitude ψ: $\{v_{x1} \sim \sin(t'), v_{y1} \sim \cos(t'), B_{x1} \sim \cos(t'), B_{y1} \sim \sin(t'), \rho_1 \sim \cos(t'), v_{z1'} \sim \sin(t')\}$.

We now assume the above time-dependence for all six variables and remove the relevant factors of $\sin(t')$ or $\cos(t')$ from the linear equations. Eliminating the time-dependence in this way, the first-order MHD equations reduce to a set of six interrelated first-order ordinary differential equations for the vertical structure of the disc:

$$v_{x1} - 2v_{y1} = -\frac{1}{\rho_0} d_{z'}\rho_0 + \frac{B_{z'}^2}{\rho_0}\left(d_{z'}B_{x1} - \frac{\rho_1}{\rho_0} d_{z'}B_{x0} - B_{x0} d_{z'}B_{x0}\right), \tag{52}$$

$$-v_{y1} = -(2-q)v_{x1} + \frac{B_{z'}^2}{\rho_0} d_{z'}B_{y1} - v_{z1'} d_{z'} v_{y0}, \tag{53}$$

$$v_{z1'} = 2v_{y0} - \frac{1}{\rho_0} d_{z'}\rho_1 + \frac{\rho_1}{\rho_0^2} d_{z'}\rho_0 + \frac{B_{z'}^2}{\rho_0}\Big(- B_{x0} d_{z'}B_{x1} - B_{x1} d_{z'}B_{x0} + B_{x0} d_{z'}B_{x0}\frac{\rho_1}{\rho_0} + d_{z'}B_{x0}\Big), \tag{54}$$

$$-\rho_1 + d_{z'}(\rho_0 v_{z1'}) = 0, \tag{55}$$

$$-B_{x1} = d_{z'}v_{x1} - v_{z1'} d_{z'}B_{x0} - B_{x0} d_{z'} v_{z1'}, \tag{56}$$

$$B_{y1} = d_{z'}v_{y1} - qB_{x1}. \tag{57}$$

The symmetry properties of the first-order problem can be found by the following considerations. It was shown in Section 3.1.2 that all physical quantities have a symmetry under the transformation $\{t' \to t' + \pi, z' \to -z'\}$. Given that the zeroth-order terms have no time-dependence and the first-order terms have a sinusoidal dependence, one can deduce whether each variable is an even or odd function of z'. For example $\rho_1(-z', t' + \pi) = \rho_1(z', t')$ from the point symmetry of the warped disc, but the sinusoidal time-dependence of ρ_1 implies that $\rho_1(z', t' + \pi) = -\rho_1(z', t')$. We may thus conclude that $\rho_1(-z', t') = -\rho_1(z', t')$, or ρ_1 is an odd function of z'. In summary, $\{\rho_0, v_{y0}, v_{z1'}, B_{x1}, B_{y1}\}$ are even functions of z', while $\{B_{x0}, \rho_1, v_{x1}, v_{y1}\}$ are odd functions of z'. These symmetry considerations lead to boundary conditions (58)–(63).

Equations (52)–(57) specify six first-order differential equations with one free dimensionless parameter, $B_{z'}$, which fixes the strength of the magnetic field. This is the same dimensionless parameter used in the study of jet launching from isothermal discs by Ogilvie (2012). In addition we require six boundary conditions in order to construct a numerical solution for the vertical structure of the disc. Symmetry considerations imply that the equations need only be solved above the mid-plane and immediately fix three boundary conditions at the mid-plane. The magnetic field at the upper surface must be prescribed, leading to a further two boundary conditions (58)–(59).

We chose to impose a rigid lid on the upper disc surface corresponding to the final boundary condition (63). An analysis of the far-field solution of equations (52)–(57) implied that the high-density region of the disc is insensitive to any reasonable boundary condition on the disc outflow at sufficiently large z'. Numerical tests (see Section 5.1) confirmed this result, validating our choice of boundary condition.

In summary the boundary conditions on the problem are

$$B_{x1}(\infty) = A, \tag{58}$$

$$B_{y1}(\infty) = B, \tag{59}$$

$$\rho_1(0) = 0, \tag{60}$$

$$v_{x1}(0) = 0, \tag{61}$$

$$v_{y1}(0) = 0, \tag{62}$$

$$v_{z1}(\infty) = 0, \tag{63}$$

where A and B are the limiting values of the radial and toroidal field far above the disc mid-plane. In the context of this model, A and B are free parameters. Physically, A and B need to be determined by solving for the global magnetic field in the force-free region far above and below the disc and solving for the disc's internal structure in a self-consistent manner. Such a problem is global in character and hence beyond the scope of this work, although we will discuss it in a forthcoming publication concerned with bending equilibrium magnetic field configurations.

3.3 The magnetic field and physical relevance

Having reduced the MHD equations to a set of linear one-dimensional equations, it is informative to step back and consider the structure of the magnetic field described by this model. Due to the time dependence we have assigned to the magnetic field, the field must be anchored within the disc. Were the magnetic field not anchored within the disc, the differential rotation would inevitably lead to far more complex magnetic field configurations. Beyond being anchored in the disc, we have chosen to model the equilibrium magnetic field as purely poloidal. This assumption is made for mathematical simplicity and also to eliminate the transport of angular momentum by ether an outflow or an exchange of magnetic torques. The extent to which the magnetic field bends is a free parameter of the model. A similar magnetic field structure can be found in Guilet & Ogilvie (2012) and Ogilvie and Livio (2001).

If the dimensionless magnetic field strength $B_{z'} \lesssim 1$ we are no longer justified in neglecting the MRI. While a more detailed discussion of the MRI is given in Section 4.3, we briefly mention that due to the neglect of the MRI, this model is of greatest relevance at plasma betas of order unity where the MRI is suppressed. Magnetic fields of this strength are often invoked to explain observed jet emissions (see e.g. Moll 2012; Ogilvie 2012; Cao & Spruit 2013; Campbell 2010).

Recent studies of protostellar disc formation from molecular cloud core collapse by Lewis, Bate & Price (2015) and Lewis & Bate (2017) indicate that protostellar discs may form with plasma

Downloaded from https://academic.oup.com/mnras/article-abstract/477/2/2406/4942271
by University of Cambridge user
on 18 June 2018

betas of order unity. In addition, the continued study of magnetically arrested discs (Narayan, Igumenshchev & Abramowicz 2003) around black holes further motivate the study of strongly magnetized warped disc dynamics. It is in this strong regime that the results of this paper are most applicable.

4 THE SPECIAL CASE OF THE PURELY VERTICAL MAGNETIC FIELD

4.1 Solution via a spectral method

The simplest magnetized warped disc model is one in which the inclination angle $\tan i$ of the magnetic field at the disc boundary is zero, implying the magnetic field above and below the disc is perpendicular to the disc surface. This corresponds to setting boundary conditions (49), (58), and (59) to zero. This model is relatively easy to analyse, yet demonstrates many of the qualitative differences between purely hydrodynamic and magnetized warped discs.

Under these conditions, the unwarped density profile is given by

$$\rho_0(z') = \frac{1}{\sqrt{2\pi}} \mathrm{e}^{-z'^2/2} \tag{64}$$

and the first-order equations reduce to

$$\frac{\mathrm{d}^2 v_{x1}}{\mathrm{d}z'^2} = -\frac{\rho_0}{B_{z'}^2}(v_{x1} - 2v_{y1} - z'), \tag{65}$$

$$\frac{\mathrm{d}^2 v_{y1}}{\mathrm{d}z'^2} = \frac{\rho_0}{B_{z'}^2}(2v_{x1} - (1+2q)v_{y1} - qz'). \tag{66}$$

The coupled pair of differential equations (65) and (66) were solved via a spectral method as outlined below.

Using the set of basis functions $\{y_n(z') = P_{2n-1}(\tanh z')\}$, the first 12 eigenvalues and eigenfunctions of the following Sturm–Liouville problem were found via a combined Rayleigh–Ritz and Gram–Schmidt procedure:

$$\frac{\mathrm{d}^2 u}{\mathrm{d}z'^2} + \mu\rho_0 u = 0, \tag{67}$$

where we impose the boundary conditions $u(0) = 0$ and $\frac{\mathrm{d}v}{\mathrm{d}z'} = 0$ at large z'. Let this eigenfunction basis be $\{u_i\}$, with associated eigenvalues $\mu_i = \{3.363, 22.30, 57.12, 107.8, \dots\}$. The eigenfunctions u_i are plotted in Fig. 3 (see also Latter, Fromang & Gressel (2010)).

Equations (43) and (44) together with a vanishingly small magnetic field perturbation at large z' imply that velocity perturbations v_{x1} and v_{y1} must have a vanishingly small derivative at the upper boundary. Through symmetry arguments one can deduce that v_{x1} and v_{y1} are odd in z' and so vanish at $z' = 0$. Therefore, v_{x1} and v_{y1} satisfy the same boundary conditions as the eigenfunctions u_i. Let us project the velocity perturbations v_{x1}, v_{y1} and the function $f(z') = z'$ on to this basis in the following way:

$$v_{x1}(z') = \sum_i a_i u_i(z'), \tag{68}$$

$$v_{y1}(z') = \sum_i b_i u_i(z'), \tag{69}$$

$$z' = \sum_i c_i u_i(z'). \tag{70}$$

Projecting the function z' on to the eigenfunction basis $\{u_i\}$ requires some consideration, as this function does not satisfy the appropriate boundary conditions far from the mid-plane. However, beyond a few scale heights the density becomes vanishingly small and the error in approximating z' via the set of eigenfunctions $\{u_i\}$ is negligible.

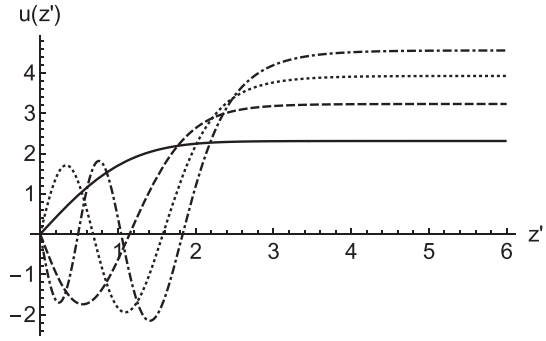

Figure 3. The first four eigenfunctions of equation (71), u_1, u_2, u_3, u_4. The velocities of the Alfvénic-epicyclic modes are proportional to these eigenfunctions.

If we let $\lambda_i = \mu_i B_{z'}^2$, the MHD equations (65)–(66) give

$$a_i = -\frac{\lambda_i - 1}{\lambda_i^2 - 2(1+q)\lambda_i + (2q-3)} c_i, \tag{71}$$

$$b_i = \frac{\lambda_i q + 2 - q}{\lambda_i^2 - 2(1+q)\lambda_i + (2q-3)} c_i, \tag{72}$$

where

$$c_i = \int_0^\infty z' \rho_0(z') u_i(z')\, \mathrm{d}z'. \tag{73}$$

The critical aspect of this set of equations is the dependence of the denominator on the magnetic field strength and the shear rate q associated with the disc. Resonances will occur whenever either of the following conditions holds for any eigenvalue μ:

$$B_{z'}^2 \mu = 1 + q + \sqrt{4 + q^2}, \tag{74}$$

$$B_{z'}^2 \mu = 1 + q - \sqrt{4 + q^2}. \tag{75}$$

These resonances result in arbitrarily large velocities, magnetic fields, and internal torques acting within the disc. More generally equations (71)–(73) imply the existence of a set of modes, henceforth called Alfvénic-epicyclic modes, in this magnetized warped disc. They are the result of a coupling between the magnetic field and the epicyclic modes. Each of these modes is associated with its own distinct vertical structure and a natural frequency given by

$$\omega_{i(\mathrm{fast})}^2 = \lambda_i + 2 - q + \sqrt{4\lambda_i + (2-q)^2} \tag{76}$$

and

$$\omega_{i(\mathrm{slow})}^2 = \lambda_i + 2 - q - \sqrt{4\lambda_i + (2-q)^2}. \tag{77}$$

Whenever there is a coincidence between the natural frequency of a particular Alfvénic-epicyclic mode and the orbital frequency ($\omega = 1$ in scaled units), a resonance will occur and that mode will dominate the solution.

The Alfvénic-epicyclic mode velocities are proportional to their respective eigenfunction u_i, while the magnetic field strengths associated with each mode are proportional to the derivatives of the respective eigenfunction $\frac{\mathrm{d}u_i}{\mathrm{d}z'}$. The radial and azimuthal velocities for the first and second Alfvénic-epicyclic modes are shown in Table 1. The absolute magnitude of these velocities becomes arbitrarily high

Downloaded from https://academic.oup.com/mnras/article-abstract/477/2/2406/4942271
by University of Cambridge user
on 18 June 2018

Table 1. The vertical structure of the first two Alfvénic-epicyclic fast and slow modes. The radial and toroidal velocity perturbations v_{x1} and v_{y1} are represented in the left-hand column by the solid and dashed lines, respectively. The magnetic field perturbations B_{x1} and B_{y1} are represented in the right-hand column by the solid and dashed lines respectively. In all cases $q = 1.6$ and the magnetic field is varied to be close to the resonant points of the first two Alfvénic-epicyclic fast and slow modes. Referencing from the top row down, the resonances shown correspond to the first slow mode, the first fast mode, the second slow mode, and the second fast mode. The associated magnetic field strengths are shown on the left of each row.

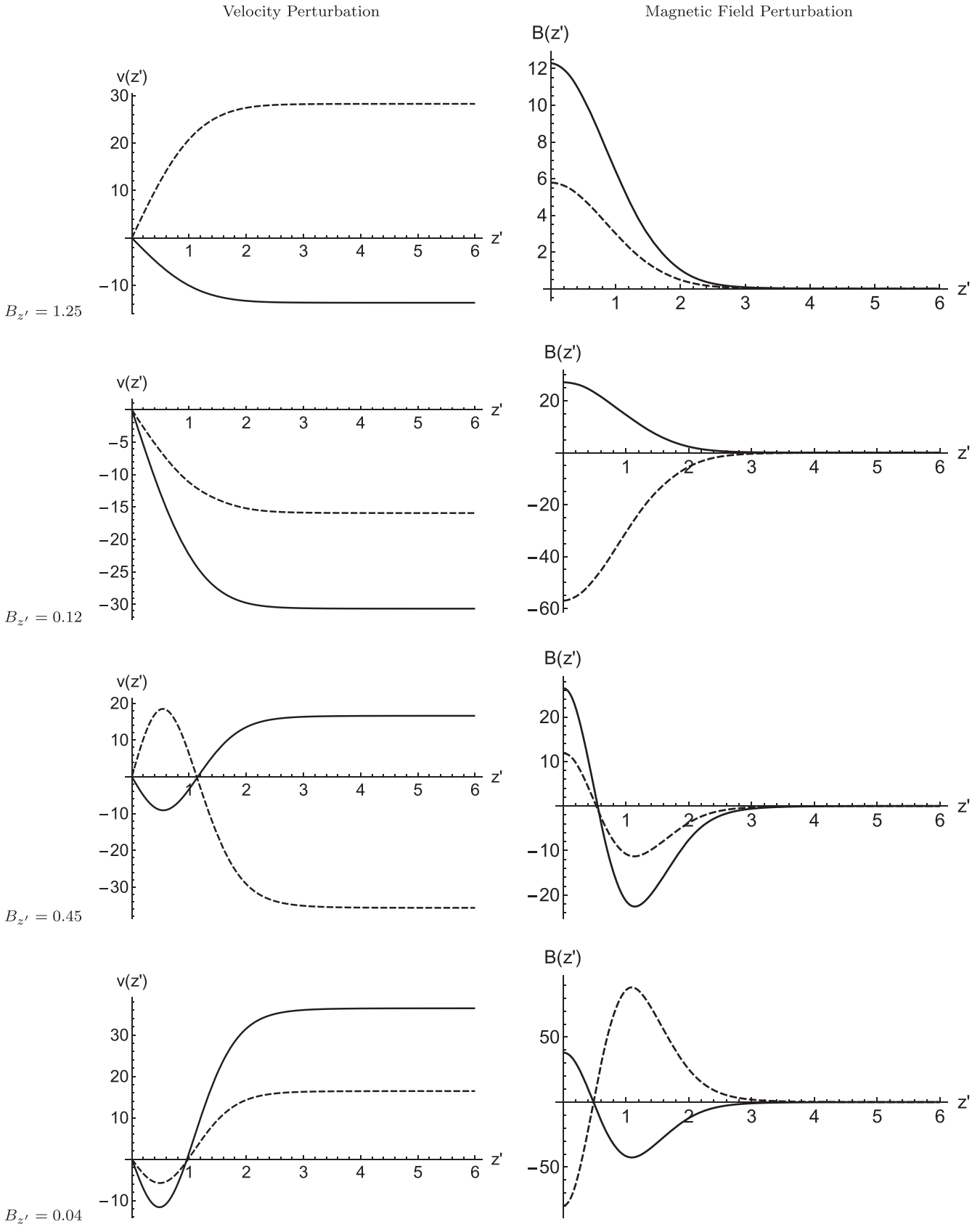

Downloaded from https://academic.oup.com/mnras/article-abstract/477/2/2406/4942271
by University of Cambridge user
on 18 June 2018

as a resonance is approached, leading to a breakdown of the linear formalism outlined here. An investigation into the fully non-linear theory would be required to explore the behaviour near resonance.

In the Keplerian case ($q = 3/2$), which is the case of greatest physical interest, equations (74)–(75) reduce to

$$B_{z'}^2 \mu_i = 5, \tag{78}$$

$$B_{z'}^2 \mu_i = 0, \tag{79}$$

implying that the fast modes are all resonant iff $B_{z'} = 0$. This corresponds to the hydrodynamic resonance familiar from earlier work. On the other hand, if the strength of the magnetic field is non-zero this resonance will be lifted and, provided the orbital frequency does not coincide with the natural frequency of a slow Alfvénic-epicyclic mode, well-behaved solutions are obtained. The magnetic field strengths associated with these resonances of the slow modes are at $B_{z'} = \{1.22, 0.473, 0.296, 0.215, \ldots\}$, the resonances becoming more and more closely spaced as the magnetic field strength approaches zero.

4.2 The internal torque

The internal structure of a magnetized disc with an external magnetic field oriented normal to the disc surface was found in the previous section. The torque acting on the disc can now be calculated. As found in Ogilvie & Latter (2013a), the torque acting within the disc may be written in the following way:

$$\boldsymbol{G} = -2\pi \Sigma c_s^2 r^2 \left(Q_1 \boldsymbol{l} + Q_2 r \frac{\partial \boldsymbol{l}}{\partial r} + Q_3 r \boldsymbol{l} \wedge \frac{\partial \boldsymbol{l}}{\partial r} \right), \tag{80}$$

where Q_1, Q_2, and Q_3 are dimensionless coefficients given by

$$-Q_1 \Sigma c_s^2 = \left\langle \int (\rho v_x v_y - T_{xy})\, \mathrm{d}z' \right\rangle_{t'}, \tag{81}$$

$$-Q_4 \psi \Sigma c_s^2 = \left\langle \mathrm{e}^{\mathrm{i}t'} \int [\rho v_x(-\Omega z' - \mathrm{i} v_z) + \mathrm{i} T_{xz}]\, \mathrm{d}z' \right\rangle_{t'}, \tag{82}$$

where $Q_4 = Q_2 + iQ_3$. The angular brackets denote that the quantities inside the brackets are time-averaged. Q_1 is similar to the usual accretion disc torque, while Q_2 corresponds to diffusion of the warp and Q_3 causes a dispersive wave-like propagation of the warp.

Torque coefficients Q_1 and Q_2 are related to dissipation. This model does not include viscosity or resistivity, implying both of these coefficients will vanish and only Q_3 need be considered. We note that this can be also be proven by considering the symmetry properties of the system as discussed in Section 3.1.2.

Equation (82) suggests that a radial magnetic stress T_{xz} will contribute to Q_3; for a vertical equilibrium field configuration however, this radial stress is exactly balanced by a magnetic stress difference above and below the disc surface. The contribution to the torque from magnetic stresses is therefore of order $O(h/r)$ relative to the angular momentum flux, and is assumed to be small. Only the radial flux of angular momentum need be considered, implying that

$$Q_3 = \frac{1}{2\pi} \int_0^{2\pi} \int \rho_0 v_{x1} z' \sin^2 t' \mathrm{d}z' \mathrm{d}t' + O(\psi^2). \tag{83}$$

Projecting v_{x1} and z' on to the eigenfunction basis $\{u_i\}$ described above in (67) and using the orthogonality relationships of the eigenfunction basis, equation (83) simplifies to

$$Q_3 = \sum_i \frac{(1-\lambda_i)}{\lambda_i^2 - 2(1+q)\lambda_i + (2q-3)} c_i^2, \tag{84}$$

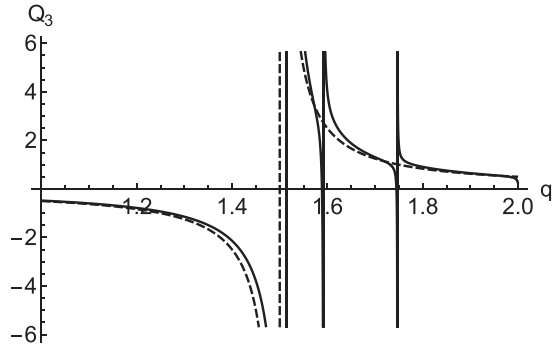

Figure 4. The internal torque coefficient Q_3 as a function of q at magnetic field strength $B_{z'} = 0.04$. The dotted line shows Q_3 for a hydrodynamic disc. The discontinuities at $q > 1.5$ correspond to resonances of fast Alfvénic-epicyclic modes.

where $\lambda_i = \mu_i B_{z'}^2$. In the hydrodynamic limit, recalling that normalization of density implies $\sum c_i^2 = 1/2$, we find

$$Q_3 = \frac{1}{2(2q-3)} + O(\psi^2, B^2), \tag{85}$$

which is consistent with the result found by Ogilvie & Latter (2013a) for a hydrodynamic warped disc.

The internal torque coefficient Q_3, as can be seen by the denominator of equation (84), also diverges near an Alfvénic-epicyclic resonance. The dependence of Q_3 on the magnetic field strength $B_{z'}$ and shear rate q is shown in Figs 4–8. The Alfvénic-epicyclic resonances as functions of q and $B_{z'}$ are shown in Fig. 9 for comparison.

It is worthy of note that in the strong-field limit $B_{z'}^2 \gg 1$, $Q_3 \approx \frac{-c_1^2}{\mu_1 B_{z'}^2}$. At very large magnetic field strengths the increasing stiffness imbued by the magnetic flux dampens the disc response. Consequently the induced internal flows lower in amplitude and warp propagation slows as the magnetic field strength is increased.

The weak field limit is far more subtle. Since the model presented in this paper is concerned with mean-field effects, it is reasonable to expect that at weaker field strengths the hydrodynamic limit for Q_3 is recovered. It can be seen in Fig. 4 that this holds true at all points except those very near to an Alfvénic-epicyclic resonance. At these resonances the warp structure and propagation properties may be quite sensitive to the magnetic field strength and even a relatively weak magnetic field may have significant consequences for the warp evolution. This has special physical relevance in light of the fact that a hydrodynamic Keplerian disc is precisely at one such resonance (or alternatively, the resonance of a Keplerian hydrodynamic disc could be considered as the pile-up of fast Alfvénic-epicyclic modes as the magnetic strength falls to zero as shown in Fig. 8). Warp propagation in a Keplerian low-viscosity disc may therefore be quite sensitive to the introduction of even a weak magnetic field. In the Keplerian weak-field limit $B_{z'}^2 \ll 1$, the case of most physical interest, we note that $Q_3 \approx \frac{-c_1^2}{5\mu_1 B_{z'}^2}$.

In a more realistic model one might expect the mean-field effects described above to compete with viscous effects including those that might arise from MRI turbulence. In some circumstances, these non-ideal effects may eliminate any distinction between the MHD model presented here and the corresponding hydrodynamic model. Further investigation is required to determine what factors influence warp propagation in a weakly magnetized disc.

Although viscosity has not been included in any of the derivations thus far, let us consider the effect of a magnetic field on the internal

Downloaded from https://academic.oup.com/mnras/article-abstract/477/2/2406/4942271
by University of Cambridge user
on 18 June 2018

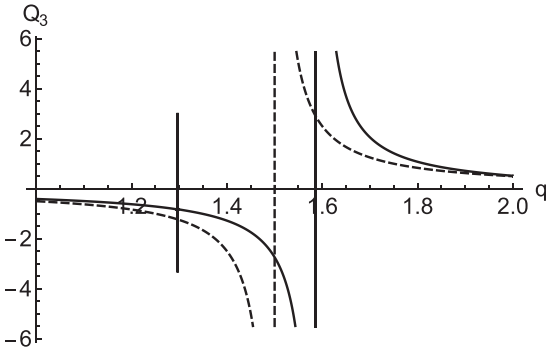

Figure 5. The internal torque coefficient Q_3 as a function of q at magnetic field strength $B_{z'} = 0.1$. The central discontinuity originally at $q = 1.5$ has been displaced rightward, lifting the hydrodynamic resonance at q=1.5.

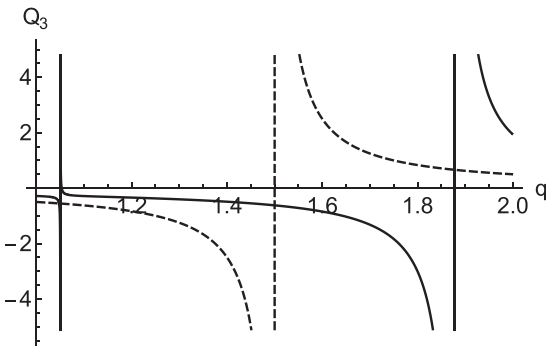

Figure 6. The internal torque coefficient Q_3 as a function of q at magnetic field strength $B_{z'} = 0.2$. The central discontinuity has moved well past $q = 1.5$. Near $q = 1.0$ there is a discontinuity associated with a slow Alfvénic-epicyclic mode.

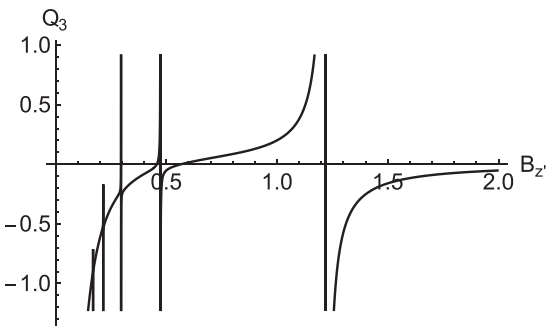

Figure 7. The internal torque coefficient Q_3 as a function of magnetic field strength $B_{z'}$ in scaled units for a Keplerian disc. The most significant resonance occurs at $B_{z'} = 1.22$, corresponding the ground state Alfvénic-epicyclic mode.

torque coefficient Q_2. It was found in Ogilvie & Latter (2013a) that the torque coefficient Q_2 in a Keplerian disc grows inversely with viscosity as the hydrodynamic resonance is approached. It is expected, subject to further analysis, that the presence of a magnetic field will lift the resonance of a Keplerian hydrodynamic disc and therefore remove the divergence in torque coefficient Q_2, reducing the anomalously quick diffusion of the warp in this case.

We would like to emphasize for completeness that it is only for the vertical equilibrium field configuration that there is no explicit magnetic contribution to the torque. Warp propagation in discs with a 'bending' field ($B_{x0} \neq 0$) differs from the vertical field case in several respects. Notably, the magnetic field can potentially play a greater role in the transport of angular momentum through the disc. We refer the reader to an upcoming paper for details of warp propagation in more general magnetic field configurations.

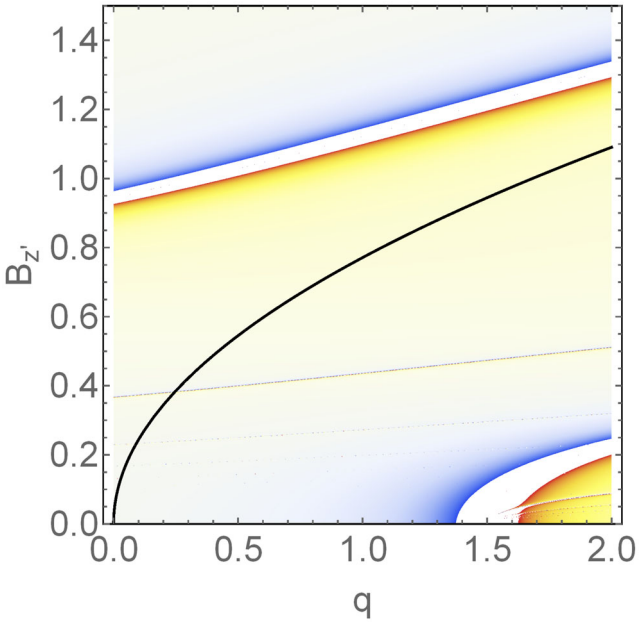

Figure 8. Torque coefficient Q_3 as a function of shear rate q and magnetic field strength $B_{z'}$. White regions indicate large torques that fall beyond the plot range. Due to poor resolution, many of the higher order resonances are not clearly visible. Large values of Q_3 can be observed near the first slow mode resonance where $B_{z'} \approx 1$ and near the first fast mode resonance. The fast mode resonance is responsible for the anomalous behaviour of Keplerian hydrodynamic warped discs. The MRI stability curve is shown in black.

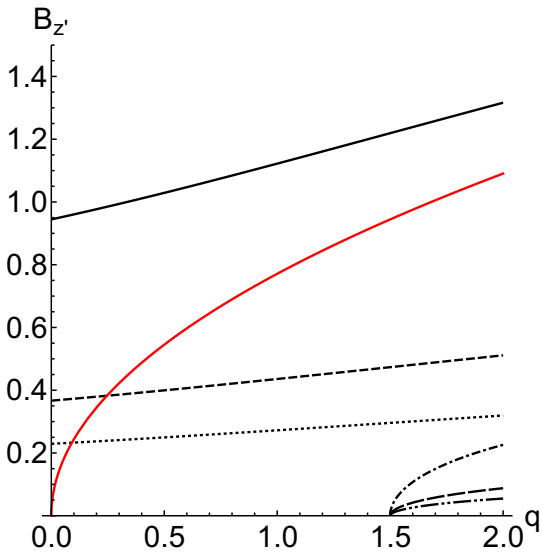

Figure 9. The Alfvénic-epicyclic resonances in the q–$B_{z'}$ plane. The first three slow resonances are the top three nearly straight lines in this figure. The bottom three curves, with a common meeting point at $q = 3/2$ for the hydrodynamic case, are the first three fast Alfvénic-epicyclic resonances. The MRI stability curve is shown in red.

Downloaded from https://academic.oup.com/mnras/article-abstract/477/2/2406/4942271
by University of Cambridge user
on 18 June 2018

4.3 Effects of the MRI

The MRI in an accretion disc can be expected to exist for a range of magnetic field strengths $B_{\min} < B_{z'} < B_{\max}$. The upper limit of the MRI-unstable region $B_{\max}$ may be found by a standard analysis of the ideal MHD equations as first derived in Balbus & Hawley (1991). It is informative to note the connection between their analysis and the analysis presented here. While investigations of the MRI are primarily focused on the unstable normal modes of a magnetized accretion disc, the chief focus of this work has been the resonant forcing of stable modes. However, when the natural frequency of a stable Alfvénic-epicyclic mode transitions from a real to an imaginary number, that mode becomes unstable corresponding to the onset of the MRI. From equation (64) one can deduce that this transition will occur when

$$\mu_1 B_{z'}^2 = 2q, \tag{86}$$

where μ_1 is the smallest of the eigenvalues defined by equation (67). In the case of a vertical magnetic field and a Keplerian disc, we can conclude that

$$B_{\max}^2 = \frac{q}{1.68}. \tag{87}$$

Though formulated slightly differently, this corresponds exactly to the result found by Gammie & Balbus (1994) for isothermal discs.[2] Given that the resonance associated with the lowest order eigenfunction of equation (54) occurs for a Keplerian disc at $B_{z'} \approx 1.22$ while the MRI is expected below $B_{z'} \approx 0.94$, one can see that a large-scale magnetic field may have a significant effect on the warp dynamics even in the MRI stable region. This is an important result because if it was discovered that the resonances discussed in the previous chapters only existed in the MRI unstable region $B_{z'} < B_{\max}$, one would be uncertain as to whether these resonances are likely to exist once the effects of the MRI are taken into account.

There are a few shortcomings with the analysis above. First, we found an identical MRI stability condition to that found by Gammie & Balbus (1994). This is unsurprising as the MRI has emerged as an instability in our linear perturbation of an unwarped disc state. Non-linear warped disc solutions may not have the same MRI stability conditions and require a non-linear analysis beyond the scope of this work. Secondly, the value of $B_{\max}$ found is only valid for the particular vertical magnetic field configuration considered in this section. Using the numerical methods outlined in section 4, we hope to analyse the MRI stability condition for a disc with an equilibrium bending magnetic field ($B_{x0} \neq 0$).

For small magnetic field strengths, the question is significantly more complicated. The value of $B_{\min}$ is related to the non-ideal behaviour of the disc, and therefore is beyond the scope of this analysis. It is unclear at this stage what effects MRI turbulence would have on disc structure or warp propagation.

4.4 Comparison with hydrodynamic warped discs

It is instructive to consider briefly how the magnetized warped disc considered here relates to the hydrodynamic warped disc discussed in Ogilvie & Latter (2013a).

The distinctive characteristics of a hydrodynamic warped disc are largely due to the unbalanced pressure gradient in the radial equation of motion due to the warped geometry. Internal flows therefore must exist in a warped hydrodynamic disc. More specifically, linear flows were shown to be valid solutions. These flows will be resonantly driven for a Keplerian disc owing to the coincidence of the epicyclic and orbital frequencies. This leads to the rapid diffusion of the warp at small viscosities.

In contrast to a hydrodynamic disc, such simple linear flows are no longer solutions for the internal disc structure of a magnetized warped disc. The presence of the magnetic field adds some stiffness to the fluid, detuning the epicyclic frequency from the orbital frequency and thereby lifting the resonance. In more detail, it was found that there are a number of fast and slow Alfvénic-epicyclic modes present with no analogue in the hydrodynamic disc. These modes may resonate if their natural frequency coincides with the orbital frequency, effectively driving a resonant response.

In an ideal inviscid disc the only non-zero internal torque coefficient is Q_3. The properties of Q_3 may be dramatically different from those of the corresponding hydrodynamic problem, reflecting the far richer structure of the magnetized warped disc. It is also expected that due to the detuning of the epicyclic and orbital frequencies in a warped magnetized disc, the anomalously large values of Q_2 found in the hydrodynamic Keplerian case will be reduced.

At progressively weaker field strengths (see Fig. 4) the difference between the MHD solution and the corresponding hydrodynamic solution becomes negligible except when the disc is very close to an Alfvénic-epicyclic resonance. Near these resonances the internal structure is very sensitive to small changes in parameters and the magnetohydrodynamic perturbations may have a significant effect on disc structure. This is of some physical relevance as a hydrodynamic Keplerian disc corresponds to one such resonance, and consequently may be sensitive to the introduction of a relatively weak magnetic field. Further investigation is required to probe the weak field limit and the effects of the MRI or a finite viscosity.

5 NUMERICAL SOLUTIONS

5.1 Solution via numerical ODE solver

In the previous section, we described in detail a semi-analytical solution to the ideal MHD equations of a warped disc without mass outflow in the specific case where, at large distances, the external magnetic field is perpendicular to the disc surface. In this section, we outline a numerical method for solving for the internal structure of an accretion disc. There are two motivations for this. First, this provides a check on the semi-analytical results outlined in the previous section. Secondly, it would allow us to solve for the structure of the disc for a more general equilibrium magnetic field configuration and with more general boundary conditions. The method developed is outlined below.

In Section 3.2.2, we derived a set of six first-order ordinary differential equations for the six first-order variables; these are given by equations (52)–(57). The six necessary boundary conditions were also given in equations (58)–(63). In Section 3.3.1, we derived three first-order equations for structure of the unwarped equilibrium disc, along with the three associated boundary conditions.

Owing to symmetry considerations our range of integration may be restricted to $0 < z' < z_h$, where z_h is the effective upper surface of the disc and is some number of scale heights above the mid-plane. z_h was chosen to be small enough such that the numerical methods described remain feasible, yet large enough to be considered exterior to the disc for all practical purposes. All results were tested at various values of z_h to ensure that its value did not have a significant impact.

[2] We are in agreement with the general form for the Alfvén velocity at the mid-plane, $V_{0z}^2 > 2q\Omega_0^2 H^2/E_1$, as well as the lowest order non-zero eigenvalue $E_1 \approx 1.34$. However, we do not agree on the exact stability condition $V_{0z}^2 > 0.45c_s^2$ that they quote for $q = 3/2$.

Downloaded from https://academic.oup.com/mnras/article-abstract/477/2/2406/4942271
by University of Cambridge user
on 18 June 2018

The boundary conditions were satisfied via the shooting method. The nine variables were integrated from the mid-plane to the upper surface of the disc. Four of the nine boundary conditions fix the value of a variable at the mid-plane, requiring the value of the five remaining variables at the mid-plane to be guessed. The Newton–Raphson method was employed to refine these five initial value guesses and satisfy the five boundary conditions at the upper surface. All results were found to be insensitive to subsequent iterations of the Newton–Raphson method and all boundary conditions were satisfied to an acceptable degree of error, leading to the conclusion that the Newton–Raphson method had converged on a valid solution.

There are four free parameters in this numerical system. One is $B_{z'}$, a constant which determines the relative strength of the magnetic field in the system. The remaining three are the boundary conditions on the magnetic field which specify the connection between the magnetic field within the disc region and the magnetic field of the disc exterior. The first is $B_{x0}(z_h)$, determining the angle of the equilibrium poloidal field to the disc surface. The remaining two are $B_{x1}(z_h)$ and $B_{y1}(z_h)$, the first-order radial and toroidal magnetic fields external to the disc. These four free parameters must be specified to solve for the internal structure of the disc.

As discussed in Section 3.3.2, one of the boundary conditions on this system of equations was the imposition of a rigid lid corresponding to equation (63). Based on a far-field analysis of the linear MHD equations, it was found that the results in the high-density region of the disc should be insensitive to the exact value of the outflow velocity. This was tested by varying the outflow velocity at the upper surface. We confirmed that the rigid lid had little effect on our solutions.

All numerical results found via this method were consistent with the results of the semi-analytical calculation described in Section 4 to a reasonable degree of accuracy.

5.2 The corrugated sheet model

As an alternative to the approach outlined here, one may also consider a standard shearing box model within which all perturbed variables vary sinusoidally with radius at a specified wavenumber k (giving a thin disc the appearance of a corrugated sheet). For very small k this corresponds exactly to the model presented above, where the warping is assumed to be independent of the radius. A numerical setup similar to the Runge–Kutta ODE solver outlined above was used for this corrugated sheet model. This model is informative because it allows us to investigate the dispersion relation $\omega(k)$ of radial bending waves. While the details of this model will be discussed in an upcoming paper, there are two results highly relevant to the work presented here.

First, the torque coefficient Q_3 can be found from the quadratic dispersion relation of the normal modes of the unwarped magnetized disc. In an unwarped disc there exists a normal mode with frequency $\omega(0) = \Omega$ (where Ω is the orbital frequency) corresponding to vertical oscillations of the disc. For small but non-zero radial wavenumber k, the frequency of this mode is related to Q_3 via

$$\omega(k) = \Omega + Q_3 \frac{c_s^2}{\Omega} k^2. \tag{88}$$

It was found that the torque coefficients Q_3 obtained by this numerical method were consistent with the semi-analytical calculations presented in Section 4, providing a valuable check on our results.

Secondly, $\omega(k)$ at the critical points in the $(B_{z'}, q)$ plane corresponding to Alfvénic-epicyclic resonances were investigated. We found that the warp dispersion relation transitions from quadratic to linear near these critical points. This transition implies a qualitative change in the disc behaviour associated with enhanced warp propagation at these points. This result, described in more detail in the relevant upcoming paper, perhaps most clearly illustrates the physical interpretation of a divergent torque coefficient Q_3.

6 SUMMARY AND DISCUSSION

Using the warped shearing box framework set out by Ogilvie & Latter (2013a), the local ideal MHD equations were found for warped magnetized thin discs. These equations were expanded to terms linear in the warping parameter ψ. While a general analysis of the solutions to these equations is forthcoming, the case of an external magnetic field oriented normal to the disc surface is relatively simple and can be solved semi-analytically via a spectral method. The results of this analysis were verified by the use of a numerical ODE solver. Many of the distinct characteristics of warped magnetized discs may be illuminated by this rather simple model.

In a hydrodynamic disc it was found that the coincidence of the epicyclic and orbital frequencies causes a resonance in thin Keplerian accretion disc models. This resonance results in fast internal flows and torques acting within the disc, resulting in the rapid propagation of the warp.

In the presence of a magnetic field this resonance is removed. The magnetic tension adds a stiffness to the epicyclic oscillations, detuning the epicyclic frequency from the orbital frequency. Therefore at low viscosities the presence of even a relatively weak magnetic field may dramatically alter the internal structure of a Keplerian or very nearly Keplerian warped disc and evolution of the warp.

In magnetized warped discs there exists a series of normal modes which we have called Alfvénic-epicyclic modes. These are the normal modes of the magnetized accretion disc, each with a fixed vertical structure and phase relationship between the density, velocity, and magnetic field perturbations. For a vanishing magnetic field, the fast Alfvénic-epicyclic modes all oscillate at the orbital frequency while the slow modes are static ($\omega = 0$), thereby recovering the results found by Ogilvie & Latter (2013a). The frequencies of the Alfvénic-epicyclic modes depend on the shear rate q, the magnetic field strength and the inclination of the equilibrium magnetic field.

The warped geometry of the accretion disc creates a pressure gradient in the radial direction that acts as an inhomogeneous forcing term. This system is consequently analogous to a forced oscillator. When the frequency of an Alfvénic-epicyclic mode coincides with the orbital frequency, that particular mode is resonantly forced resulting in large internal torques and rapid warp propagation. Warp propagation in magnetized discs consequently has a surprisingly subtle and rich dependence on the magnetic field strength and shear rate. This mechanism may be critical to understanding and modelling warp propagation in magnetized discs.

In this paper, we have assumed that there is no jet outflow from the disc. The effect of disc warping on jet outflows is not well understood and could be studied using the framework set out in this paper. We also hope to use the methods developed in this paper to investigate accretion discs with a wider variety of magnetic boundary conditions corresponding to more general magnetic field orientations.

The solutions investigated in the latter half of this paper have neglected the MRI. Consequently, the results of those sections are expected to be of greatest validity in highly magnetized discs ($\beta \approx 1$). The MRI, and especially the interplay between the MRI and the warped magnetized accretion disc dynamics outlined in this paper, could also be investigated using the formalism developed here.

Downloaded from https://academic.oup.com/mnras/article-abstract/477/2/2406/4942271
by University of Cambridge user
on 18 June 2018

ACKNOWLEDGEMENTS

This work was funded by the Science and Technology Facilities Council (STFC) through a studentship to J. Paris and through grant ST/L000636/1.

REFERENCES

Agapitou V., Papaloizou J. C. B., Terquem C., 1997, MNRAS, 292, 631
Balbus S. A., Hawley J. F., 1991, ApJ, 376, 214
Bardeen J. M., Petterson J. A., 1975, ApJ, 195, L65
Blandford R. D., Payne D. G., 1982, MNRAS, 199, 883
Campbell C. G., 2010, MNRAS, 401, 177
Cao X., Spruit H. C., 2013, ApJ, 765, 149
Fragile P. C., Blaes O. M., Anninos P., Salmonson J. D., 2007, ApJ, 668, 417
Gammie C. F., Balbus S. A., 1994, MNRAS, 270, 138
Guilet J., Ogilvie G. I., 2012, MNRAS, 424, 2097
Hatchett S. P., Begelman M. C., Sarazin C. L., 1981, ApJ, 247, 677
Krolik J. H., Hawley J. F., 2015, ApJ, 806, 141
Lai D., 1999, ApJ, 524, 1030
Latter H. N., Fromang S., Gressel O., 2010, MNRAS, 406, 848
Lewis B. T., Bate M. R., 2017, MNRAS, 467, 3324
Lewis B. T., Bate M. R., Price D. J., 2015, MNRAS, 451, 288
Lovelace R. V. E., Romanova M. M., 2014, EPJ Web Conf., 64, 05003
Miyoshi M., Moran J., Herrnstein J., Greenhill L., Nakai N., Diamond P., Inoue M., 1995, Nature, 373, 127
Moll R., 2012, A&A, 548, A76
Narayan R., Igumenshchev I. V., Abramowicz M. A., 2003, PASJ, 55, L69
Nealon R., Nixon C., Price D. J., King A., 2016, MNRAS, 455, L62
Ogilvie G. I., 1997, MNRAS, 288, 63
Ogilvie G. I., 1999, MNRAS, 304, 557
Ogilvie G. I., 2012, MNRAS, 423, 1318
Ogilvie G. I., Latter H. N., 2013a, MNRAS, 433, 2403
Ogilvie G. I., Latter H. N., 2013b, MNRAS, 433, 2420
Ogilvie G. I., Livio M., 2001, ApJ, 553, 158
Papaloizou J. C. B., Lin D. N. C., 1995, ApJ, 438, 841
Papaloizou J. C. B., Pringle J. E., 1983, MNRAS, 202, 1181
Sheikhnezami S., Fendt C., 2015, ApJ, 814, 113
Sorathia K. A., Krolik J. H., Hawley J. F., 2013a, ApJ, 768, 133
Sorathia K. A., Krolik J. H., Hawley J. F., 2013b, ApJ, 777, 21
Terquem C., Papaloizou J. C. B., 2000, A&A, 360, 1031
Zhuravlev V. V., Ivanov P. B., Fragile P. C., Morales Teixeira D., 2014, ApJ, 796, 104

This paper has been typeset from a TEX/LATEX file prepared by the author.

Downloaded from https://academic.oup.com/mnras/article-abstract/477/2/2406/4942271
by University of Cambridge user
on 18 June 2018